www.saltworkconsultants.com

Salty Matters

John Warren - Sunday June 30, 2018

Stable isotopes in evaporite systems: Part III - $\delta^{18}O$ (Oxygen)

Introduction

Oxygen isotope determinations in evaporitic sediments are typically based on: 1) using oxygen held in the water molecule itself (H_2O); 2) oxygen in the carbonate anion held in evaporitic dolomites or limestones or; 3) in sulphate from evaporitically precipitated gypsum or anhydrite. Oxygen measures on the water molecule can be co-associated with deuterium (D - heavy hydrogen) determinations. So isotopic sampling of evaporitic limestone and dolomites means carbon isotope values can be co-determined from the same mineral phase (CO_3 source). Likewise, with the calcium sulphates, the sulphur isotope is always available for co-study (SO_4 source in gypsum or anhydrite).

We have already discussed sulphur and carbon isotope variations in evaporitic settings in the previous two articles (30 April 2018 and 31 May 2018, respectively). So, in this article, we shall look at how oxygen isotope values vary with the co-associated deuterium, carbon and sulphur isotope phases. We focus on three sources for isotope samples (water molecules in a brine, evaporitic carbonate minerals, calcium sulphate minerals) and show that when oxygen values are co-plotted against deuterium, carbon or sulphur isotope values, it becomes a handy tool in defining depositional and diagenetic evolution in a range of evaporitic settings.

Oxygen isotope fractionation in water molecules in evaporating brines

The stable isotope community has long known of the potentially extreme effects of evaporation on the isotopic composition of liquids and the residual enrichment of the heavier isotope in the remaining brine. After all, Urey himself applied this knowledge when he demonstrated the existence of deuterium through evaporative enrichment of liquid hydrogen (Urey et al., 1932). Enrichment in heavier isotopes in the residual brine is documented in settings as diverse as evaporating Dead Sea brines (Gat, 1984) and degassing epithermal systems (Zheng, 1990).

As any water (brine) evaporates there is a commensurate preferential escape of the lighter ^{16}O water molecules, this leaves behind an increasing proportion of heavier water molecules containing ^{18}O. Hence, with increasing degrees of evaporation the $\delta^{18}O$ signature in the remaining water mass becomes increasingly positive (Figure 1). Co-variance of deuterium with increasing oxygen isotope values

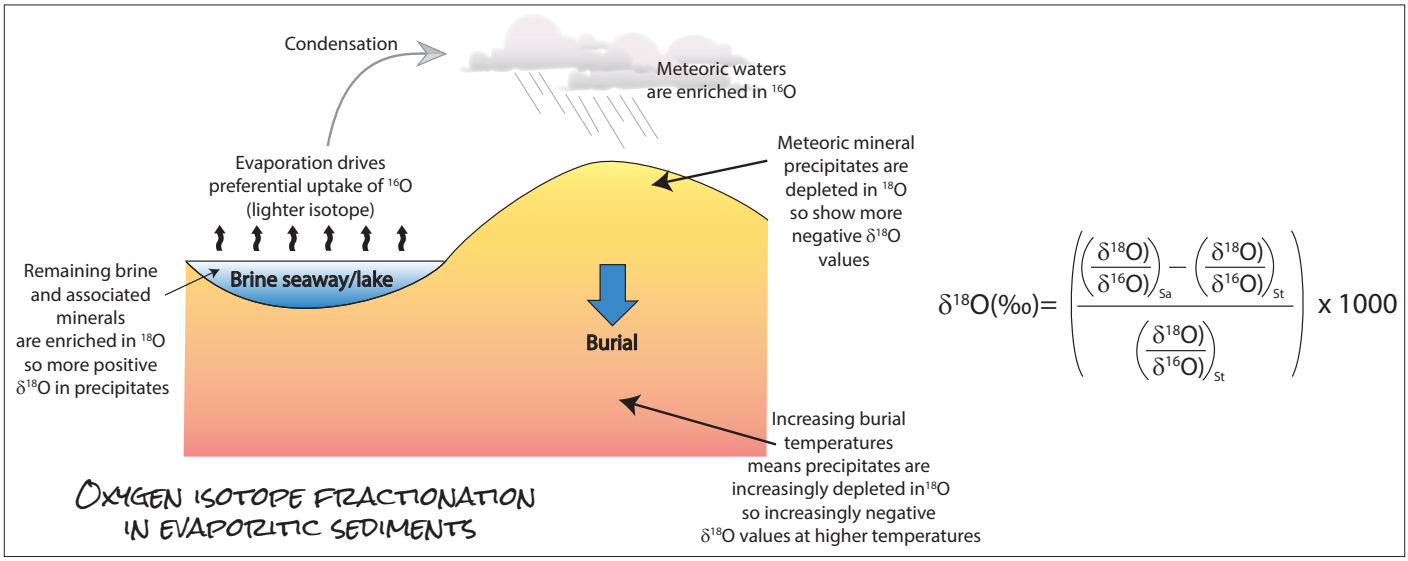

Figure 1. Controls on the enrichment of heavier isotope in residual brine and depletion in atmospheric water and subsequent rainfall and infiltrating groundwaters (meteoric water).

in a concentring brine is a long-established observation (Figure 2; Cappa et al., 2003), and defines a type of Raleigh fractionation or distillation.

There is another factor involved in the degree of enrichment of the heavier isotopes of oxygen or deuterium, and that is the humidity of the air above the evaporating brine. Humidity controls the extent of evaporative concentration, and there is a differential level of isotope enrichment in the residual brine tied to changing humidity (Figure 2). It is a response to the lowering of the evaporation rate with increasing humidity. The humidity effect in evaporative settings is documented both experimentally and in natural settings such as modern sabkhas and salinas (Chapter 2 in Warren 2016, for a summary of literature). As a general rule, the lower the humidity, the greater the degree of enrichment of the heavier isotope. Horton et al., (2016) show that $\delta^{18}O_{SMOW}$ values of saline lake waters from are often shifted by >+10‰ relative to source waters discharging into the lake (Figure 3, especially 3c).

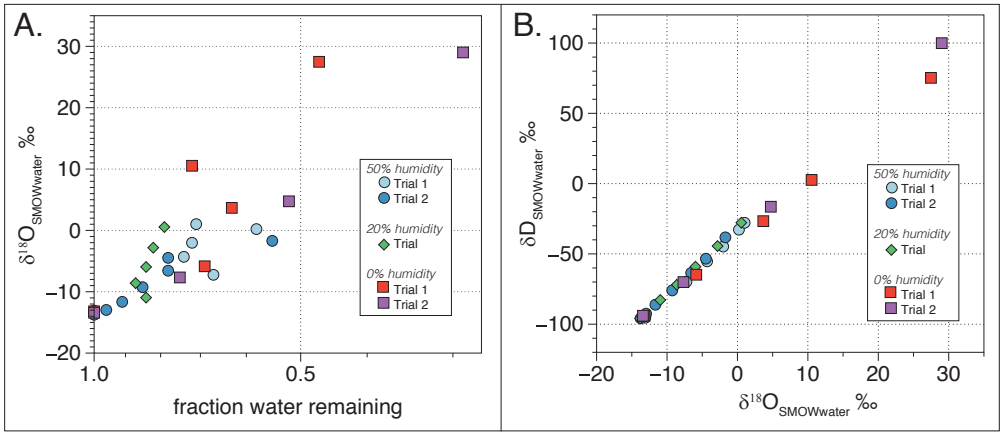

Figure 2. Heavy isotope enrichment through evaporation A) Evolution of d18O over the course of an evaporation experiment plotted against remaining brine fraction at three humidity levels. For each humidy level the results (trial) plot in a linear fashion. The isotopic ratios approach steady state as f_0. B) The δD versus $\delta^{18}O$ (liquid) values for each experiment. A linear relationship is observed with a best fit to all the data of D = 4.34$\delta^{18}O$ - 35.8. (replotted from Cappa et al., 2003).

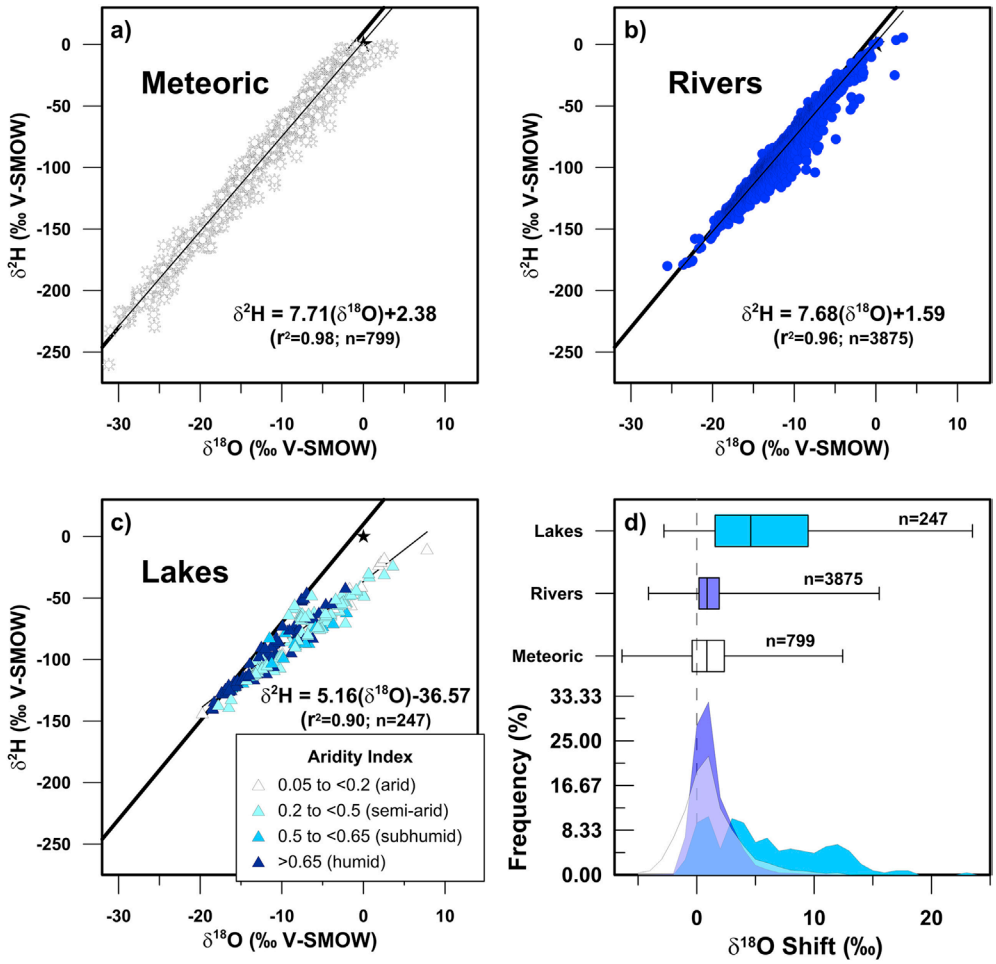

Figure 3. δ^2H and $\delta^{18}O$compositions compiled western North America meteoric (A), river (B) and lake (C) waters (from Horton et al., 2016). Regional stable isotopic water line equations represent the least-squares linear regression fits through all data points plotted in each panel. Black star represents standard mean ocean water (SMOW) and thick black line represents the global meteoric water line (GMWL). Lake water symbols in panel C are color coded according to the modern aridity index at each sampling site. Panel D shows frequency distributions and whisker-box plots of the $\delta^{18}O$ shift away from the global meteoric water line along an evaporation line of slope 4.5 for each sample type. Vertical lines in the whisker-box plots (Panel D) represent, minimum, lower quartile, median, upper quartile, and maximum $\delta^{18}O$ shift values observed.

Up until February 1979, the Dead Sea was a permanently stratified hypersaline water body (see Warren 2016, Chapter 4 for hydrological and sedimentological details). Both the upper and lower water masses were moderately enriched in $\delta^{18}O_{SMOW}$ (Figure 4: Gat 1984). After the overturn and mixing the surface waters, the degree of enrichment in $\delta^{18}O$ in the surface waters constitutes a balance between the dilution by freshwater influx and the isotope fractionation (enrichment) which accompanies evaporative water loss and vapour exchange with the atmo-

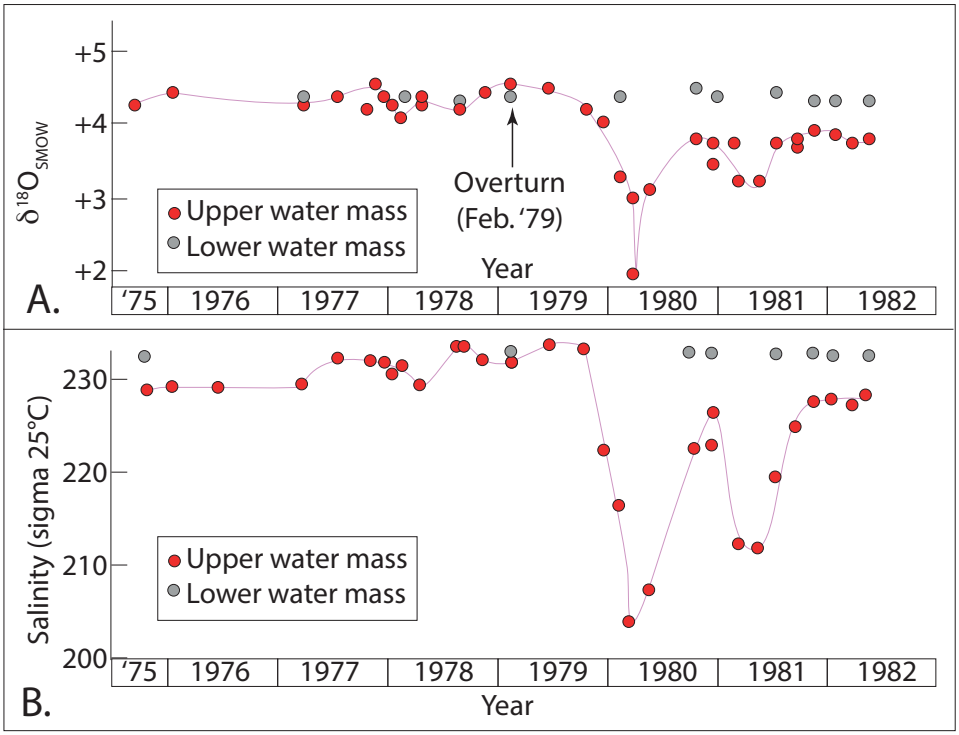

Figure 4. Dead Sea, Middle East (after Gat, 1984). $^{18}O_{SMOW}$ over time (A) and salinity (B) values for surface and deep waters in the yeats 1975-1982. Salinity is given in sigma-25 units ($\sigma_t = (\rho_t - 1) \times 10^3$) where ρ is the density of the solution and t = 25°C)

spheric moisture. Gat's modelling of the seasonal cycle and long-term trends of $\delta^{18}O_{SMOW}$ in response to the changes in the environmental parameters, shows that the dominant control on isotope enrichment in the surface waters, post overturn, is exercised by the salinity of the surface waters, through its effect on the vapour pressure gradient between the lake's surface and the atmosphere. Interestingly, before the overturn event the upper water mass was more homogenous in terms of salinity and isotope enrichment and its enriched isotope values mostly tracked those of the much more stable and somewhat more saline lower water mass.

Deuterium-oxygen isotope plots of water molecules can also be useful in studying the origin of hydrated salts such as gypsum, but only if there has been minimal postdepositional alternation of the primary precipitate. A classic paper focusing on the composition of structural water held in the gypsum lattice of Messinian (Late Miocene) evaporites of Sicily was published by Bellanca et al., 1986. In Sicily, there are two main types of texture in gypsum-dominated outcrops in the Messinian sub-basins of Sicily (laminated and massive). The laminar gypsum, locally known as balatino, is a shallow-water saltern deposit, the other is a massive form of gypsum typically interpreted as a diagenetic replacement of either primary gypsum of anhydrite.

The different isotopic compositions of hydration water in the two gypsum lithotypes are shown in Figure 6. Laminar gypsum shows a predominance of positive values for both oxygen (range -1.59‰ < $\delta^{18}O_{SMOW}$ < +6.02‰) and deuterium (range -7.3‰ < δD < +22.7‰), while both oxygen and deuterium ranges in the massive gypsum are negative (-4.21‰ < $\delta^{18}O_{SMOW}$ > -2.23‰; -40.9‰ < δD < -34.4‰).

In Figure 5 the majority of points representative of the laminar gypsum mother waters fall to the right of the meteoric water line of Craig (1961) and lie on a path characterised by a positive slope ($\delta D = 3.97\delta^{18}O_{SMOW} - 0.59$) and includes the SMOW point. Such a distribution is consistent with an origin of the gypsum by direct precipitation from an evaporating solution saturated with respect to gypsum and is close to those of mother waters in recent gypsum samples precipitated in Mediterranean salinas and, therefore, suggest that the solutions from which the laminar gypsum precipitated were marine waters concentrated by evapo-

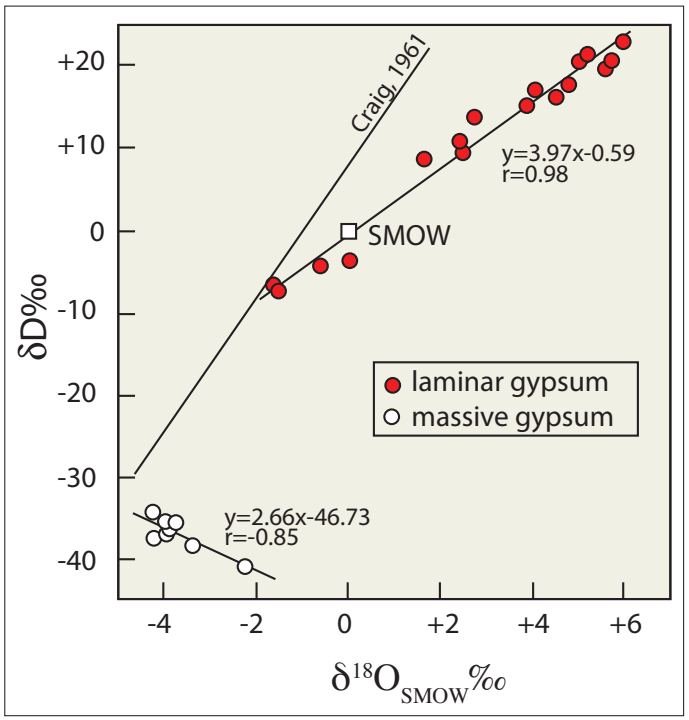

Figure 5. Oxygen and hydrogen isotopic compositions (versus V-SMOW) of hydration waters in laminar and massive gypsum (after Bellanca et al., 1986. For comparison, the meteoric water line (established by Craig 1961) is plotted

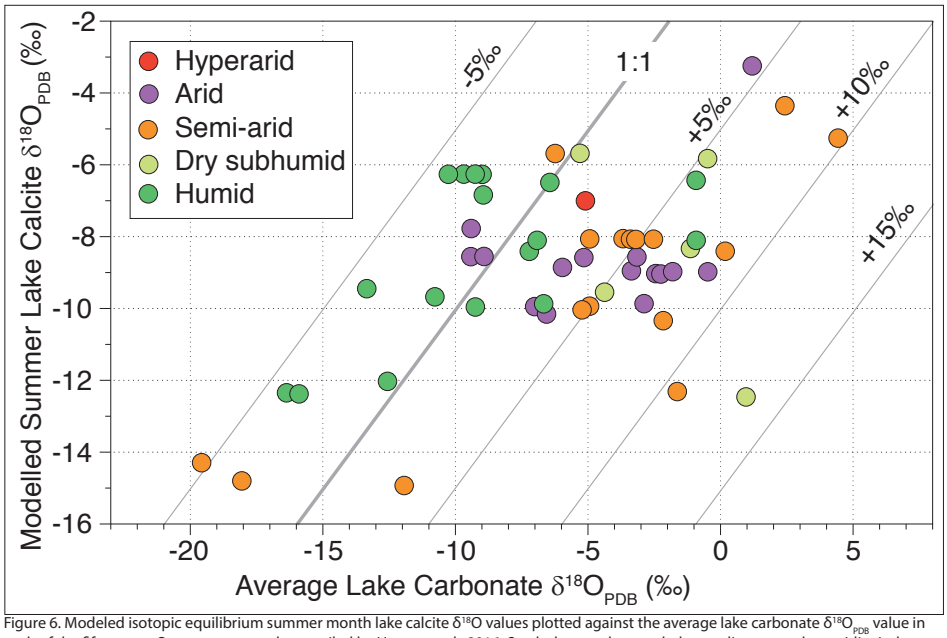

Figure 6. Modeled isotopic equilibrium summer month lake calcite $\delta^{18}O$ values plotted against the average lake carbonate $\delta^{18}O_{PDB}$ value in each of the fifty-seven Quaternary records compiled by Horton et al., 2016. Symbols are colour-coded according to modern aridity index

Figure 6. Modeled isotopic equilibrium summer month lake calcite $\delta^{18}O$ values plotted against the average lake carbonate $\delta^{18}O_{PDB}$ value in each of the fifty-seven Quaternary records compiled by Horton et al., 2016. Symbols are colour-coded according to modern aridity index values. Solid grey line represents a 1:1 (i.e. no difference) relationship. Labeled lighter grey lines correspond to -5‰, +5‰, +10‰ and +15‰ ^{18}O depletion/enrichments in observed lake carbonate isotopic composition relative to modelled summer lake calcite compositions.

ration. A few other examples show $\delta^{18}O$ and δD values shifted towards negative values, which indicate stages of dilution with large masses of continental waters poured into the deposition basin during the crystallisation of gypsum (Bellanca et al., 1986).

In contrast, the waters from Massive Gypsum plot along a line with a negative slope (δD = -2.66 $\delta^{18}O_{SMOW}$ -46.73). Clearly, these structural waters have a different origin. Bellanca (op. cit) argues these distinctive signatures are indicative of rehydration from anhydrite; others argue massive gypsum is a result of subsurface recrystallisation of primary gypsum without an intervening anhydrite stage (see Testa and Lugli (2000) for the detailed discussion of this topic)

Carbon and oxygen isotope co-variations in evaporitic carbonates

The isotopic makeup of residual water molecules evolving into a brine is not the only phase affected by the chemical consequences of evaporation (Horton et al., 2016; Warren 2016). As any natural water evaporates, its chemistry changes, as concentrating dissolved phases and increasing alkalinity force changes in equilibrium conditions. One of the most obvious consequences of evaporation is the formation of sedimentary evaporites, including brine pool carbonates (e.g. calcite, aragonite, dolomite, trona). The coupled $\delta^{18}O$ and $\delta^{13}C$ enrichment during evaporation, and the precipitation of endogenic Holocene carbonates is documented and discussed at some length in a number of review papers (Horton et al., 2016; Pierre, 1988).

Horton et al. (2016) document a general tendency for calcites precipitated in lakes located in somewhat less humid climates to show enrichment in the heavier isotope. The observed average lake carbonate $\delta^{18}O_{PDB}$ values from the 57 lakes plotted in Figure 6 are more positive than the modelled summer month meteoric water derived calcite $\delta^{18}O$ values (Horton et al., 2016). Lake calcites precipitating in humid environments generally plot closer to the 1:1 line, suggesting lakes in these environments are less impacted by evaporative modification. Yet, 46 of the 57 lake records analysed (i.e. 81%) plot to the right of the 1:1 line consistent with evaporative modification of lake water $\delta^{18}O$. Forty-two percent of the lake carbonate $\delta^{18}O$ records are >5‰ shifted towards more positive $\delta^{18}O$ values than would be expected for summer-month carbonate precipitates derived from unmodified local meteoric water. Although many lakes with vastly different modern aridity index values show similar offsets between modelled and observed $\delta^{18}O$, lakes from currently arid and semi-arid environments have a much larger average $\delta^{18}O$ offset (5.4‰) than sub-humid and humid environment lakes (2.0‰).

The dolomite forming lakes of the Coorong region show a similar set of enrichment in both oxygen and carbon isotopes within that type of Holocene dolomite precipitating directly from evaporating surface brines (dolomite Type-A; Rosen et al., 1989; Warren 1990, 2000). The other type of Holocene dolomite in the Coorong lakes (dolomite-B) shows no noticeable C-O covariant trend related to Raleigh distillation (Figure 7a). Type-A dolomite has a heavier oxygen isotope signature than type-B and is 3 - 6‰ heavier in ^{13}C (Figure 7a). Type-A dolomite also has distinct unit cell dimensions (Rosen et al., 1989).

Type A tends to be magnesium-rich with up to 3-mole percent excess $MgCO_3$, while type-B is near stoichiometric or calcian-rich. Type-A dolomite typically occurs in association with magnesite and hydromagnesite, Type B with Mg-calcite. Transmission electron microscopy (TEM) shows that Type A dolomites have a heterogeneous microstructure due to closely spaced random defects, while type B dolomites exhibit a more homogeneous microstructure implying excess calcium ions are more evenly distributed throughout the lattice. TEM studies show that the two types of Coorong dolomite are distinct and are not inter-

mixed with other mineral phases; they are primary precipitates, and not replacements and are not transitional (Miser et al., 1987).

Within the lake stratigraphy the dolomites occupy two distinct positions, Type A dolomites occur as surficial 'yoghurt' textured gels that in each water-filled winter season are washed and blown across the lake surface. By late spring and through summer these surface waters have dried up (summer salinities ≈ 120‰), and the lake sediment surface is a mud-cracked interval of massive carbonate (Warren, 1990; 2016). Type B dolomites occur in the laminated unit that underlies the laminated with signatures implying precipitation from waters with bicarbonates, perhaps showing a stronger strong input from organic materials and are especially prevalent in the more marginward part of the laminated fille where meteoric groundwaters are continually flowing into the edges of the lakes and mixing with lake pore brines.

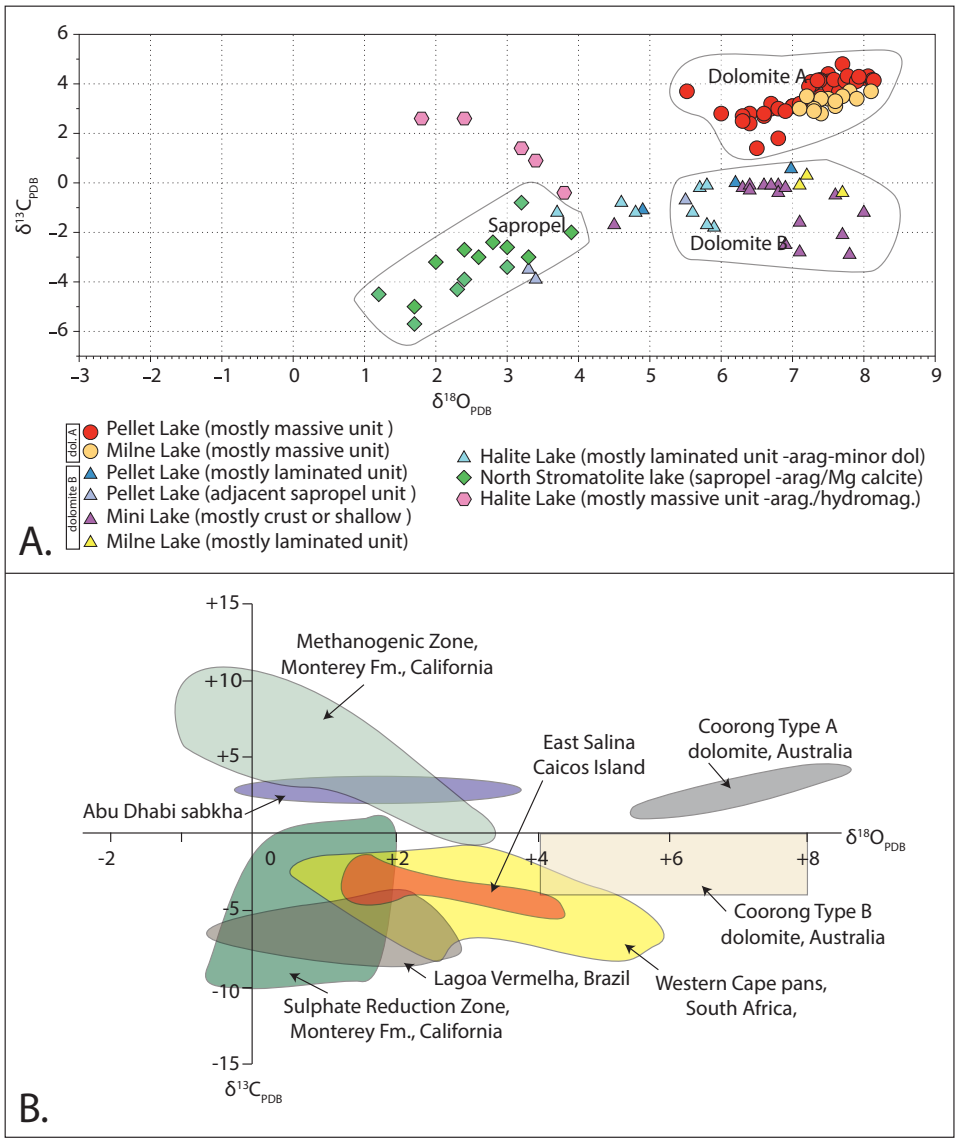

Figure 7. Carbon-oxygen isotope covariance in Holocene dolomites (after Warren, 2016). A) Isotopic signatures of Type A, Type B dolomite and sapropel carbonates across various Coorong Lakes. B) Plot fields of $\delta^{13}C_{PDB}$ versus $\delta^{13}C_{PDB}$ values for Holocene dolomites and associated minerals in various documented bacterial sulphate reduction and Archeal methanogenesis zones (after Mauger and Compton, 2012; and Warren 2000 and references therein).

Figure 7b places these two Coorong dolomites in the context of other areas of primary dolomite accumulations within Holocene carbonate depositional settings. Today sulphate-reducing bacteria or archeal methanogens have been called upon to explain the primary precipitation of dolomite in bacterial biofilms in almost all these other settings. It is not my intention to question the importance of bacterial metabolism in these other dolomite-accumulating settings, only to point out the bicarbonate from which the Coorong type A dolomites have precipitated show a positive and co-variant enrichment in both carbon and oxygen valued that are more typical of evaporative concentration. Evaporative enrichment in carbon values tied CO_2 degassing in highly saline waters was documented in the Dead Sea by Stiller et al., 1985 and discussed in last month's article (31 May 2018).

Evaporitic carbonates especially when interbedded with calcium sulphate beds can also dissolve and alter (Warren, 2016; Chapter 7). Evaporite-derived dedolomites are often associated with evaporite dissolution breccias, which indicates the stratigraphic position of the now dissolved calcium sulphate bed that supplied the excess calcium needed to dedolomitise (Lee, 1994; Fu et al., 2008). Dedolomite under this scenario forms via the reaction of calcium sulphate-rich solutions with pre-existing dolomite to produce calcite with magnesium sulphate as a possible byproduct. The latter is rarely preserved, as it is highly soluble, and either remains as dissolved ions in the escaping waters or is quickly redissolved and flushed by through-flowing groundwaters (Shearman et al., 1961). The $CaSO_4$ dissolution process is often driven by meteoric flushing of near-surface oxidising waters and former ferroan dolomites are preferentially replaced. The resulting calcitised dolomites are outlined by intervals stained red with iron oxides and hydroxides.

With uplift-related (telogenetic) dedolomites the distri-

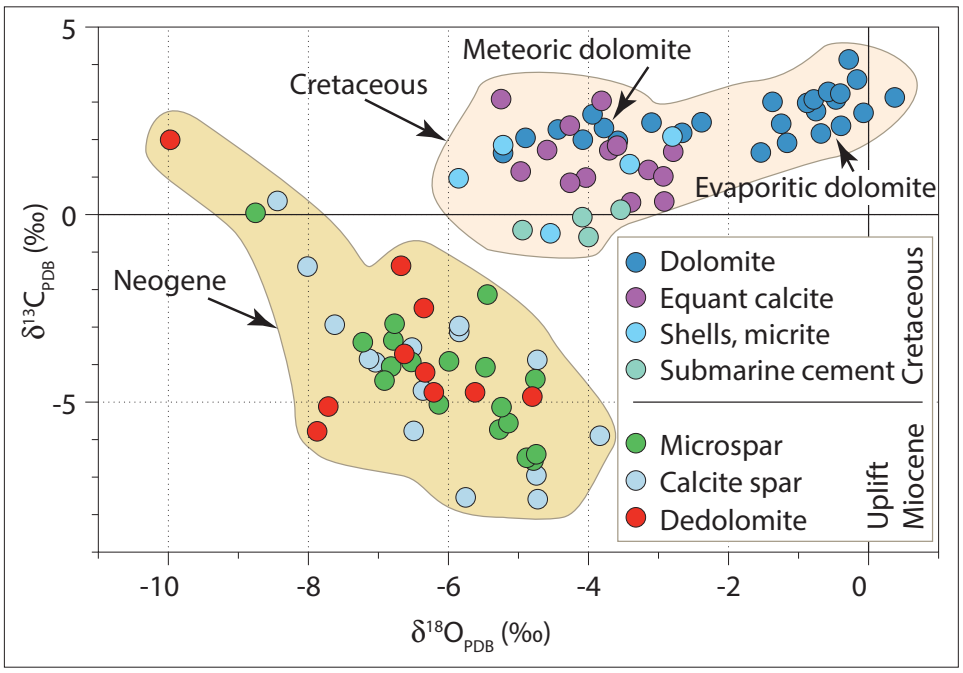

Figure 8. Crossplot of $\delta^{18}O_{PDB}$ and $\delta^{13}C_{PDB}$ of selected samples taken from the Edwards Group, Balcones fault zone, central Texas, showing two clusters related to Cretaceous digenetic overprints and Neogene telogenesis including dedolomite formed by $CaSO_4$ dissolution tied to uplift of the Edwards Plateau (replotted from data in Ellis, 1985).

bution and isotopic composition of dedolomite can reflect variations in the regional hydrology. This can be seen in the dedolomites of the Lower Cretaceous Edwards Group in the Balcones fault zone area of south-central Texas (Ellis, 1985, 1986). The Edwards Group consists of 120-180 metres of porous limestone and dolomite that accumulated on the Comanche shelf in shallow-water subtidal, intertidal, and supratidal marine environments. During early burial diagenesis, carbonate mud neomorphosed to calcitic micrite, aragonite and Mg-calcitic allochems were altered to calcite or were leached, and evaporites formed in tidal-flat sediments. Each of these phases had a characteristic stable isotope signature (Figure 8). Dolomite is widespread and formed in environments ranging from hypersaline to fresh-water as shown by the two isotope clusters in the Edwards dolomite (meteoric versus evaporitic reflux).

Late Tertiary faulting along the Balcones fault zone, tied to Jurassic salt withdrawal, initiated a circulating, fresh-water aquifer system to the west and north of a fairly distinct "bad-water line," which roughly parallels the Balcones fault zone. To the south of the bad-water line, interstitial fluids remained relatively stagnant and contain over 1000 mg/l dissolved solids. Because of the differences in the chemistry of the interstitial fluids, post-faulting diagenesis in the two zones has been very different.

Water in the bad-water zone can be saturated with respect to calcite, dolomite, gypsum, celestite, strontianite, and fluorite, whereas water in the fresh-water zone is saturated only with respect to calcite. Due to the change in water chemistry, rocks in the fresh-water zone have been extensively recrystallised to coarse microspar and pseudospar, extensive dedolomitization has occurred, and late sparry calcite cements have precipitated. This creates a suite of covariant isotope trends and clusters with the dedolomite showing a distinctive set of carbon and oxygen values relate to soil water influences indicated by calcites with more negative carbon values (Figure 8 indicated by brown shading). In contrast, rocks in the bad-water zone retain fabrics associated with pre-Miocene diagenesis, and there is little or no evidence of widespread dedolomite, indicated by pink shading in Figure 8.

The importance of meteoric diagenesis in the formation of dedolomite in shallow, subsurface telogenetic environments is illustrated by the fact that the Edwards Group had a stable mineralogy of calcite and dolomite before the circulation of fresh water began and drove the precipitation of meteoric spar, microspar and dedolomite. Isotopic values for the dedolomites follow a similar trend to those of the microspars and pseudospars. As with the microspars and pseudospars formed by the entry of telogenetic water, it can be shown that dedolomites are in isotopic equilibrium with Edwards water on a regional scale, which supports the contention that the dedolomites are still forming from crossflows of present-day formation-water (Ellis, 1985).

Sulphur and oxygen relationships in calcium sulphate

Modern seawater sulphate has a homogeneous and well-defined isotopic composition for both sulphur and oxygen:

$$^{34}S_{SO4} = +20 \pm 0.5‰ \text{ CDT}$$

$$^{18}O_{SO4} = +9.5 \pm 0.5‰ \text{ SMOW}$$

Likewise, the fractionation of sulphur and oxygen, which occurs during the transition from aqueous to the solid state of sulphate is also near constant at earth surface temperatures. For gypsum, the mean values of the isotope enrichment factor are (Pierre, 1988):

$$\delta^{34}S_{gypsum—SO4} = 1.65‰$$

and,

$$\delta^{18}O_{gypsum—SO4} = 3.5‰$$

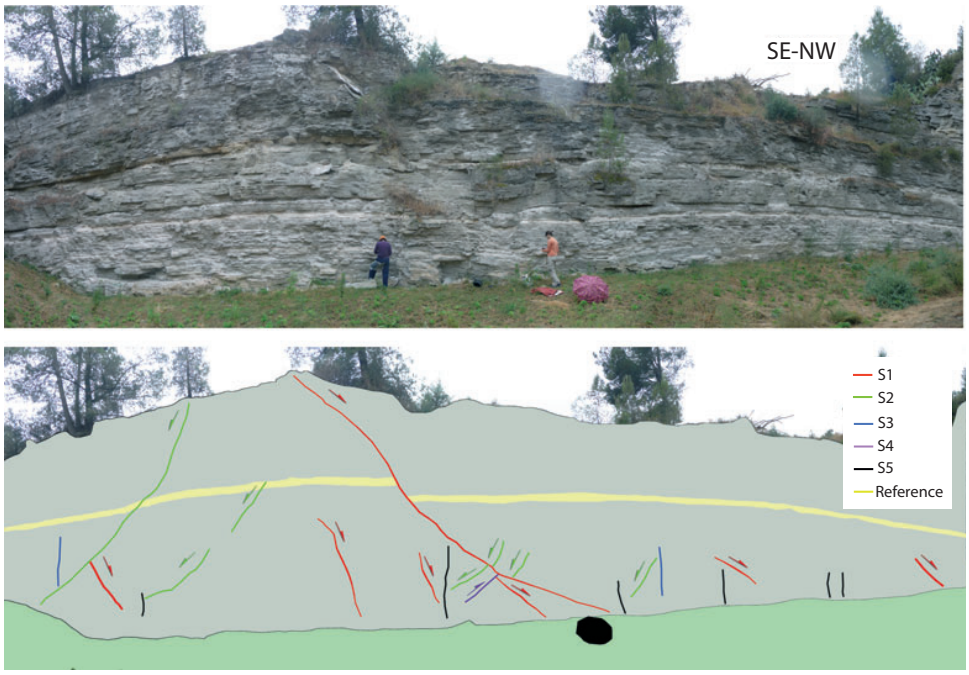

Figure 9. Outcrop panorama of the Vilobı Gypsum Unit, (Ebro Basin, Spain) in which five of the six fracture sets are highlighted. (S1 red, S2 green, S3 violet, S4 blue, S5 black (after Moragas et al., 2013)

Thus the δ34S and $\delta^{18}O$ values of sulphate evaporites are directly related to the state of the aqueous sulphate reservoir wherever precipitation occurred. A plot of ancient marine $CaSO_4$ evaporites shows the sulphur curve for seawater has varied across time from +30‰ in the Cambrian, to around +10‰ in the Permian and that it increased irregularly into the Mesozoic to its present value of +20‰. Oceanic oxygen isotope values show much less variability. Sulphur is largely resistant to isotopic fractionation during the increasing temperatures associated with burial alteration and transformation (Worden et al., 1997). All of these aspects are discussed in detail in the April 30, 2018 article.

With this knowledge of the relative lack of fractional in the subsurface compared to the much greater susceptibility of oxygen isotopes in the mesogenetic and telogenetic realms let us now look in more detail at the significance of oxygen variation in a variety of sulphate entraining settings.

Isotopically, the effects of dissolution and brine recycling in fracture-filling fibrous gypsum cements of various ages emplaced in a formation's burial evolution can be used define the sequential development of the superimposed diagenetic textures in the original gypsum unit (Figures 9, 10; Moragas et al., 2013). The upper Burdigalian Vilobí Gypsum Unit, located in the Vallès Penedès half-graben (NE Spain) and consists of a 60-m thick succession of laminated-to-banded primary and secondary gypsum. The unit is variably affected by Neogene extension in the western part of Mediterranean Sea. Tertiary extensional events are recorded in the evaporitic gypsum unit as six fracture sets and fills (faults and joints - S1 - S5), which can be linked with basin-scale deformation stages.

Combined structural, petrological and isotopic study of the unit by Moragas et al. (2013) established a chronology of fracture formation and infilling, from oldest to youngest as: (i) S1 and S2 normal faults sets with formation and precipitation of sigmoidal gypsum fibres; (ii) S3 joint sets with perpendicular fibres; (iii) S4 inverse fault sets, infilled by oblique gypsum fibres and associated with thrust-driven deformation of the previous fillings; and (iv) S5 and S6 joint sets tied to later dissolution processes and infilled by macrocrystalline gypsum cements likely related to the telogenetic realm. The fractures provided ongoing pathways for focused fluid circulation within the Vilobí Unit. The oxygen, sulphur and strontium isotope compositions of the original host rock and the various precipitates in the fractures imply ongoing convective recycling processes across the host-sulphates to the fracture infillings, as recorded by a general enrichment trend toward heavier S–O isotopes, from the oldest precip-

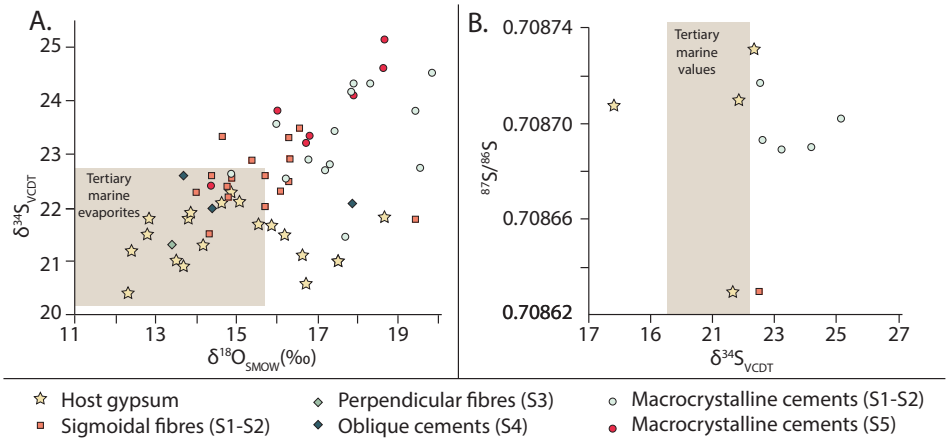

Figure 10. isotopes in the Middle Miocene Vilobi Gypsum Unit, Spain (after Moragas et al., 2013). A) $\delta^{34}S$ versus $\delta^{18}O$ cross-plot for both host gypsum rocks and various gypsum vein and fracture fills (S1-S5). B) $\delta^{34}S$ versus $^{87}Sr/^{86}Sr$ cross-plot for host gypsum, sigmoidal fibres and macrocrystalline cement samples. Shaded areas indicate plot fields for unaltered Tertiary marine evaporites.

itates (sigmoidal fibres) to the youngest (macrocrystalline cements). The marine strontium signal is mostly preserved in the various postdepositional infillings, unlike the oxygen and to a lesser extent the sulphur isotope signals, which are evolving with the origin and temperature of the waters flowing in the fracture sets (Figure 10).

In any ancient silicified anhydrite nodule or bedded silicified succession, not all silica-replacing anhydrite in a particular region need come from the same source or be emplaced by the same set of processes. Silicified nodules within middle-upper Campanian (Cretaceous) carbonate sediments from the Laño and Tubilla del Agua sections of the Basque-Cantabrian Basin, northern Spain preserve cauliflower morphologies, together with anhydrite laths enclosed in megaquartz crystals and spherulitic fibrous quartz (quartzine-lutecite). All this shows that they formed by ongoing silica replacement of nodular anhydrite (Figure 11; Gómez-Alday et al., 2002).

Anhydrite nodules at Laño were produced by the percolation of saline marine brines, during a period corresponding to a depositional hiatus. They have $\delta^{34}S$ and $\delta^{18}0$ mean values of +18.8‰ and +13.6‰, respectively, both consistent with Upper Cretaceous seawater sulphate values. Higher $\delta^{34}S$ and $\delta^{18}0$ (mean values of + 21.2‰ and 21.8‰ characterise nodules in the Tubilla del Agua section and are interpreted as indicating a partial bacterial sulphate reduction process in a more restricted marine environment (Figure 11a). Later calcite replacement and precipitation of geode-filling calcite in the siliceous nodules occurred in both sections, with $\delta^{13}C$ and $\delta^{18}0$ values indicating the participation of meteoric waters in both regions (Figure 11b). Synsedimentary activity of the Penacerrada diapir (Kueper salt - Triassic), which lies close to the Laño section, played a significant role in driving the local shallowing of the basin and in the formation of the silica in the nodules. In contrast, eustatic shallowing of the inner marine series in the Tubilla del Agua section led to the generation of morphologically similar quartz geodes, but from waters not influenced by brines derived from the groundwater halo of a diapir.

Conclusion

This and the previous two articles have underlined the utility of stable isotope samples of brine or precipitates in better understanding the origin of a range of brines and their associated precipitates. But other than the sampling of water molecules in modern brines, the interpretation of all isotope values is equivocal without a petrographic understanding of how and when the sampled textures formed. Stable isotopes of evaporitic minerals with sulphur, carbon and oxygen are the mainstays of isotope work in the study of most evaporite basins, both modern and ancient. Other isotopes that may be useful are ^{11}B and ^{37}Cl, and we shall look at their application to evaporitic sediments in a later blog.

References

Bellanca, A., and R. Neri, 1986, Evaporite carbonate cycles of the Messinian, Sicily; stable isotopes, mineralogy, textural features, and environmental implications: Journal of Sedimentary Petrology, v. 56, p. 614-621.

Cappa Christopher, D., B. Hendricks Melissa, J. DePaolo Donald, and C. Cohen Ronald, 2003, Isotopic fractionation of water during evaporation: Journal of Geophysical Research: Atmospheres, v. 108.

Ellis, P. M., 1985, Diagenesis of the Lower Cretaceous Edwards Group in the Balcones Fault Zone Area, South-Central Texas: Doctoral thesis, University of Texas - Austin, 652 p.

Ellis, P. M., 1986, Post-Miocene carbonate diagenesis of the Lower Cretaceous Edwards Group in the Balcones fault zone area, south-central Texa, in P. L. Abbott, and C. M. Woodruff, eds., The Balcones escarpment, geology, hydrology, ecology and social development in central Texas, Geological Society of America, p. 101-

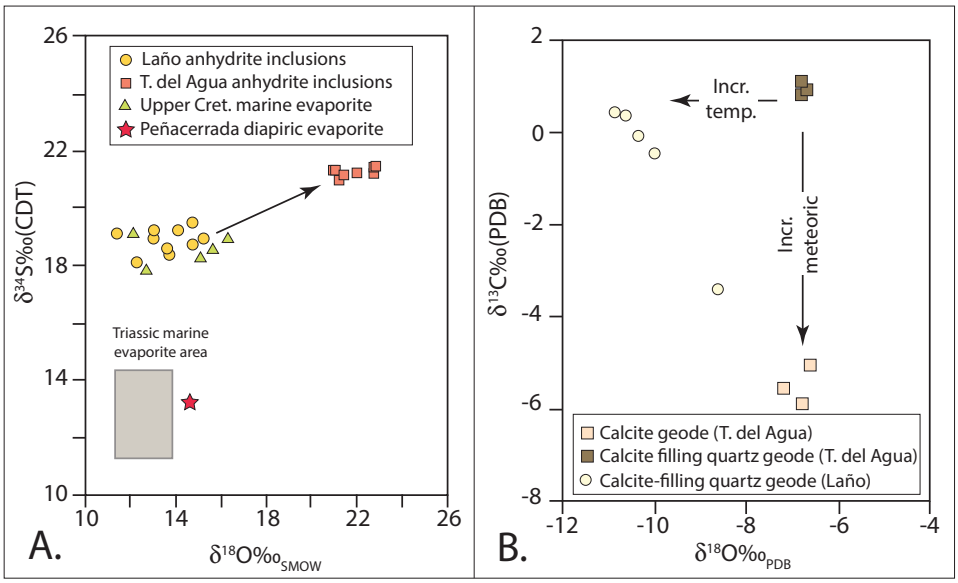

Figure 11. Stable isotopes in silicified anhydrite A) Plot of oxygen versus sulphur isotope composition of the Laño and Tubilla del Agua anhydrite inclusions together with other Triassic and Upper Cretaceous evaporite values from Spain. B) Oxygen versus carbon isotope composition of the Laño and Tubilla del Agua calcites. The Tubilla del Agua values define a vertical meteoric calcite line where the lighter ^{13}C values indicate the vadose zone while the higher values denote a phreatic zone. More negative ^{18}O values from the Laño section indicate an increase in temperature of the pore-waters.

114.

Fu, Q. L., H. R. Qing, K. M. Bergman, and C. Yang, 2008, Dedolomitization and calcite cementation in the Middle Devonian Winnipegosis Formation in Central Saskatchewan, Canada: Sedimentology, v. 55, p. 1623-1642.

Gat, J. R., 1984, The stable isotope composition of Dead Sea waters: Earth and Planetary Science Letters, v. 71, p. 361-376.

Gómez-Alday, J. J., F. Garcia-Garmilla, and J. Elorza, 2002, Origin of quartz geodes from Lano and Tubilla del Agua sections (middle-upper Campanian, Basque-Cantabrian Basin, northern Spain): isotopic differences during diagenetic processes: Geological Journal, v. 37, p. 117-134.

Horton, T. W., W. F. Defliese, A. K. Tripati, and C. Oze, 2016, Evaporation induced 18O and 13C enrichment in lake systems: A global perspective on hydrologic balance effects: Quaternary Science Reviews, v. 131, p. 365-379.

Lee, M. R., 1994, Emplacement and diagenesis of gypsum and anhydrite in the late Permian Raisby Formation, north-east England: Proceedings - Yorkshire Geological Society, v. 50, p. 143-155.

Miser, D. E., J. S. Swinnea, and H. Steinfink, 1987, TEM observations and X-ray structure refinement of a twiined dolomite microstructure: American Mineralogist, v. 72, p. 188-193.

Moragas, M., C. Martínez, V. Baqués, E. Playà, A. Travé, G. Alías, and I. Cantarero, 2013, Diagenetic evolution of a fractured evaporite deposit (Vilobí Gypsum Unit, Miocene, NE Spain): Geofluids, v. 13, p. 180-193.

Pierre, C., 1988, Application of stable isotope geochemistry to the study of evaporites, in B. C. Schreiber, ed., Evaporites and hydrocarbons: New York, Columbia University Press, p. 300-344.

Rosen, M. R., D. E. Miser, M. A. Starcher, and J. K. Warren, 1989, Formation of dolomite in the Coorong region, South Australia: Geochimica et Cosmochimica Acta, v. 53, p. 661-669.

Shearman, D. J., J. Khouri, and S. Taha, 1961, On the replacement of dolomite by calcite in some Mesozoic limestones from the French Jura: Proceedings Geological Association of London, v. 72, p. 1-12.

Shearman, D. J., J. Khouri, and S. Taha, 1961, On the replacement of dolomite by calcite in some Mesozoic limestones from the French Jura: Proceedings Geological Association of London, v. 72, p. 1-12.

Stiller, M., J. S. Rounick, and S. Shasha, 1985, Extreme carbon-isotope enrichments in evaporating brines: Nature, v. 316, p. 434.

Testa, G., and S. Lugli, 2000, Gypsum-anhydrite transformations in Messinian evaporites of central Tuscany (Italy): Sedimentary Geology, v. 130, p. 249-268.

Urey, H. C., F. G. Brickwedde, and G. M. Murphy, 1932, A Hydrogen Isotope of Mass 2: Phys. Rev., v. 39, p. 164.

Warren, J. K., 1990, Sedimentology and mineralogy of dolomitic Coorong lakes, South Australia: Journal of Sedimentary Petrology, v. 60, p. 843-858.

Warren, J. K., 2000, Dolomite: Occurrence, evolution and economically important associations: Earth Science Reviews, v. 52, p. 1-81.

Warren, J. K., 2016, Evaporites: A compendium (ISBN 978-3-319-13511-3): Berlin, Springer, 1854 p.

Worden, R. H., P. C. Smalley, and A. E. Fallick, 1997, Sulfur cycle in buried evaporites: Geology, v. 25, p. 643-646.

Saltworks Consultants Pty Ltd
ABN 068 889 127
Kingston Park,
5049 South Australia

Email: enquiries@saltworkconsultants.com

Web Page: www.saltworkconsultants.com